Centrosomal PKCβII and Pericentrin Are Critical for Human Prostate Cancer Growth and Angiogenesis

Jeewon Kim,[1] Yoon-La Choi,[3] Alice Vallentin,[1] Ben S. Hunrichs,[4] Marc K. Hellerstein,[4,5] Donna M. Peehl,[2] and Daria Mochly-Rosen[1]

Departments of [1]Chemical and Systems Biology and [2]Urology, Stanford University, School of Medicine, Stanford, California; [3]Department of Pathology, Samsung Medical Center, Sungkyunkwan University School of Medicine, Seoul, Korea; [4]Department of Molecular and Biochemical Nutrition and Metabolism, University of California, Berkeley, California; and [5]Department of Medicine, University of California, San Francisco, California

Abstract

Angiogenesis is critical in the progression of prostate cancer. However, the interplay between the proliferation kinetics of tumor endothelial cells (angiogenesis) and tumor cells has not been investigated. Also, protein kinase C (PKC) regulates various aspects of tumor cell growth, but its role in prostate cancer has not been investigated in detail. Here, we found that the proliferation rates of endothelial and tumor cells oscillate asynchronously during the growth of human prostate cancer xenografts. Furthermore, our analyses suggest that PKCβII was activated during increased angiogenesis and that PKCβII plays a key role in the proliferation of endothelial cells and tumor cells in human prostate cancer; treatment with a PKCβII-selective inhibitor, βIIV5-3, reduced angiogenesis and tumor cell proliferation. We also find a unique effect of PKCβII inhibition on normalizing pericentrin (a protein regulating cytokinesis), especially in endothelial cells as well as in tumor cells. PKCβII inhibition reduced the level and mislocalization of pericentrin and normalized microtubule organization in the tumor endothelial cells. Although pericentrin has been known to be up-regulated in epithelial cells of prostate cancers, its level in tumor endothelium has not been studied in detail. We found that pericentrin is up-regulated in human tumor endothelium compared with endothelium adjacent to normal glands in tissues from prostate cancer patients. Our results suggest that a PKCβII inhibitor such as βIIV5-3 may be used to reduce prostate cancer growth by targeting both angiogenesis and tumor cell growth. [Cancer Res 2008;68(16):6831–9]

Introduction

In the United States, prostate cancer is the third leading cause of cancer-related deaths in males (1). Although early detection and new therapies have increased survival rates, many men develop androgen-independent prostate cancers against which chemotherapeutic drugs have been generally ineffective (2). Furthermore, increases in microvessel density and expression of proangiogenic factors are associated with negative outcomes in patients with prostate cancer (3). Targeting cells that support tumor growth in addition to using cytotoxic agents to induce cancer cell death has therapeutic advantages (4–7). However, rather than targeting a single proangiogenic factor, there is a strong rationale for the development of new pharmacologic treatments that target both tumor angiogenesis and tumor cell proliferation for the treatment of prostate cancer (8).

The protein kinase C (PKC) family of serine/threonine kinases plays an important role in angiogenesis both *in vitro* and *in vivo* (9–12). Also, PKC is activated by tumor-promoting phorbol esters, and its involvement in carcinogenesis was proposed many years ago (13). Its role has because been substantiated in many human cancers, including prostate cancer (14–17). However, the role of PKC in prostate cancer angiogenesis has not been explored explicitly. Currently, a PKCβ inhibitor, Enzastaurine (a novel macrocyclic bisindolylmaleimide), is being tested in clinical trials for its antiangiogenic and anticancer effects with promising phase II studies of high-grade gliomal tumors (18). However, although the initial reports suggested that Enzastaurine is selective for PKCβ (15), subsequent studies showed that it also inhibits PKCγ, δ, and ε to a similar degree at the same concentration (14).

PKC family members are known to mediate cytokinesis and cell proliferation by microtubule regulation (19–21). Functional studies have shown a key role for pericentrin, a centrosomal protein, in microtubule organization, spindle assembly, and chromosome segregation (22, 23). Chen and colleagues (19) showed that endogenous PKCβII and pericentrin interact in K562 cells and that PKCβII colocalizes with pericentrin in G_2 and mitotic cells, i.e., dividing cells in culture. In addition, overexpression of a fragment of pericentrin that binds PKCβII leads to mislocalization of PKCβII away from the centrosome and a loss of microtubule anchoring at the centrosome, resulting in cytokinesis failure and aneuploidy. Also, overexpression of a PKCβII fragment that binds pericentrin induces the same phenotype, suggesting that increased levels of PKCβII could also disrupt interaction with pericentrin. Therefore, there is strong evidence that PKCβII and pericentrin regulate cytokinesis in cells, but the role of PKCβII and pericentrin in prostate cancer progression, both in endothelial and tumor cells *in vivo,* has not been established.

Here, we set out to determine how PKC activity affects angiogenesis and tumor cell proliferation during different stages of prostate tumor growth in a xenograft model. Our data from xenografts and patients suggest PKCβII as a target in anticancer treatment for prostate cancer against tumor-induced angiogenesis and tumor growth.

Materials and Methods

Cell lines and cell culture. PC-3 human prostate cancer cells and mouse tumor endothelial cells (TEC; 2H-11) were obtained from the American Type Culture Collection and cultured in DMEM medium with 10% fetal bovine serum (FBS; Life Technologies) with 1% antibiotics

Note: Supplementary data for this article are available at Cancer Research Online (http://cancerres.aacrjournals.org/).

Requests for reprints: Daria Mochly-Rosen, Department of Chemical and Systems Biology, Stanford University, School of Medicine, Stanford, CA 94305-5174. Phone: 650-725-7720; Fax: 650-723-4686; E-mail: mochly@stanford.edu.

doi:10.1158/0008-5472.CAN-07-6195

(penicillin and streptomycin; Life Technologies). Primary cultures of normal human epithelial cells were established from the peripheral zone of a radical prostatectomy specimen according to established techniques (24). The tissue of origin was confirmed to be normal by histopathologic analyses. Cells were cultured in a serum-free medium, "Complete PFMR-4A" (24). For *in vitro* TEC culture, 5,000 cells were seeded into each well of chamber slides in DMEM with 10% FBS and grown for 2 d in DMEM or conditioned medium from PC-3, i.e., 2-d-old medium from PC-3 cell cultures. Tumor endothelial cells were then treated with TAT (carrier peptide) or βIIV5-3-TAT at a final concentration of 1 μmol./L, thrice per day for 2 d.

Materials. For Western blot analyses, rabbit antibodies directed against Gαi-3 (C-10) were from Santa Cruz Biotechnology, Inc., and anti–glyceraldehyde-3-phosphate dehydrogenase (GAPDH) antibody, clone 6C5, was from Advanced Immunochemical. For immunofluorescence, α-tubulin and γ-tubulin Cy3 antibodies were from Sigma. Pericentrin antibodies used for immunofluorescence were from Abcam (4448). Pericentrin antibodies used for Western blot analyses (M1, 4b, and UM225) were from Dr. Stephen Doxsey (University of Massachusetts, Worcester, MA). Paraffin-embedded prostate tissues were from the Urology Department at Stanford Medical School (IRB # 348).

Peptide synthesis and administration. The PKCβII-selective inhibitor (βIIV5-3) was derived from the PKCβII V5 region [amino acids *645–650* (QEVIRN); ref. 25]. For intracellular delivery, peptides were synthesized and conjugated to a membrane-permeable TAT carrier peptide as previously described (26). TAT carrier peptide or saline was used as a control. Peptides were delivered *in vivo* using Alzet osmotic mini pumps (Alzet model 2001) as described (27). The peptides were dissolved in saline and administered at a constant rate (0.5 μL/h) corresponding to 2.4 or 24 mg/d/kg (3 or 30 mmol/L of TAT) and 3.6 or 36 mg/d/kg (3 or 30 mmol/L of βIIV5-3-TAT). Pumps were replaced every 2 wk because of the $t_{1/2}$ (~ 2 wk) of the peptides in the pump (27). Peptides were delivered for up to 5 wk.

Xenograft tumor studies. Six-week-old male nude mice were purchased from Harlan and housed at the animal care facility at Stanford University Medical Center. All mice were kept under standard temperature, humidity, and timed lighting conditions and provided mouse chow and water *ad libitum*. All animal experimentation was conducted in accordance with the Guide for Care and Use of Laboratory Animals prepared by the Institute of Laboratory Animal Resources, National Research Council, and published by the National Academy Press (revised 1996) and was approved by the Stanford University Animal Care and Use Committee. Five million PC-3 tumor cells were injected s.c. in the flank of male, 7 to 8-wk-old, athymic nude mice in sterile PBS (Fig. 1) or in a mixture of 1:1 serum-free medium and Matrigel (Becton Dickinson). Peptide treatment began when the tumors reached a group average of 100 mm^3 after ~1 week. Tumor volume (mm^3) was calculated using the equation $0.52\times$ [width (cm)]^2 $\times$ [length (cm)].

Measurement of cell proliferation. Animals were given 4% deuterated water and TECs, and tumor cells were isolated using flow cytometric sorting (refer to Supplementary Fig. S1 for cell isolation) and prepared for gas chromatography-mass spectroscopy (GC-MS) analyses as previously described (28, 29).

Immunofluorescence. Dual-color immunofluorescence was performed on fresh-frozen sections fixed in O.T.C. compound using PKC and biotin-linked rat-anti mouse CD31 antibodies (Santa Cruz Biotech, Inc. and BD PharMingen, respectively). For pericentrin and PKC detection, sections were stained with rabbit antipericentrin (ab4448; Abcam) followed by PKC antibodies. Terminal deoxynucleotidyl-transferase–mediated dUTP nick-end labeling (TUNEL) staining was carried out using an *in situ* cell death detection kit (TMR red) according to manufacturer's instructions (Roche Applied Science). Cleaved caspase-3 antibody was from Cell Signaling. CD31- and TUNEL-positive areas were measured using Photoshop (Version 9.0.1). Hoechst 333242 was from Molecular Probes. The apparatus for

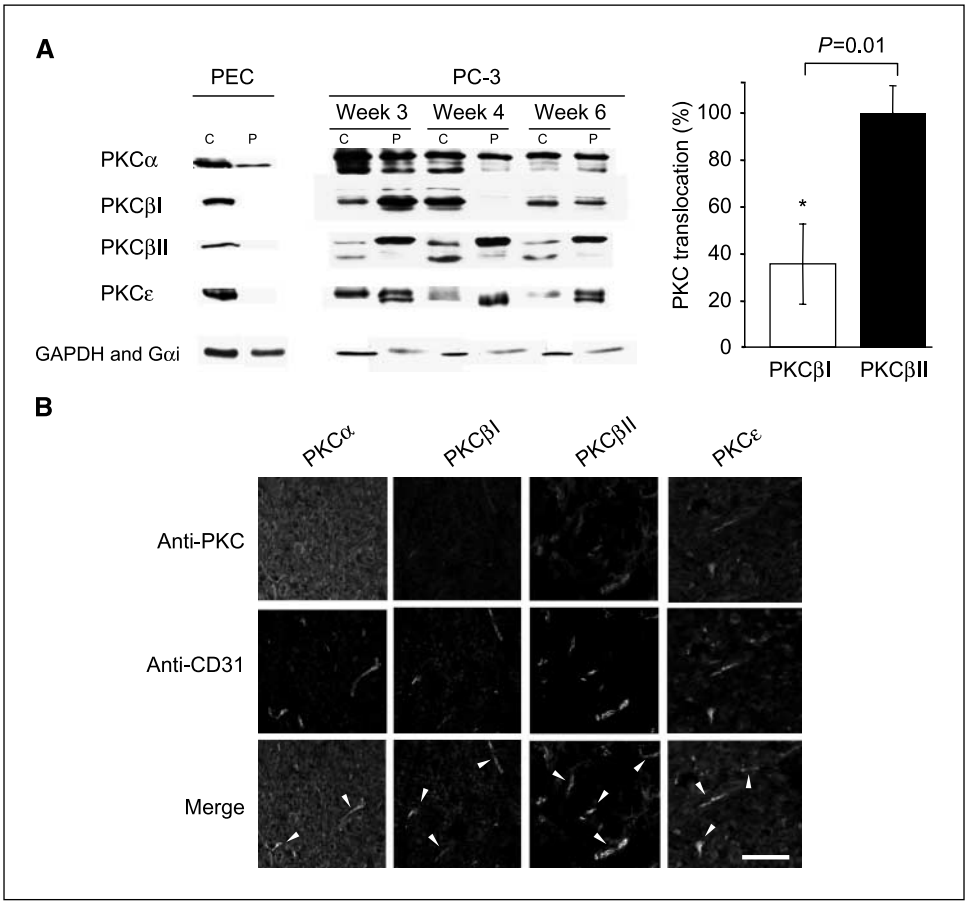

Figure 1. PKCβII is active in growing PC-3 prostate tumors and is localized mainly in tumor endothelium compared with other PKC isozymes. *A,* the level of the active form of PKC isozymes was determined by Western blot analyses of cytosolic (*C*) and particulate (*P*) fractions from 3-, 4-, and 6-wk-old tumors using anti-PKCα, βI, βII, and ε antibodies. Tumors were fractionated as described in Materials and Methods. Normal human PEC grown in serum-free medium (Complete PFMR-4A; ref. 24) without bovine pituitary extract were used to show basal levels of PKC translocation in this cell type. Quantification of the active forms of PKCβI and βII at week 6 (translocation; expressed as percentage of PKC isozyme in the particulate fraction over total cellular enzyme) is provided on the right (n = 4; *, P = 0.01). A two-tailed Student's t test was used to determine significance. Loading controls for cytosolic and particulate fractions (GAPDH and Gαi) are shown. *B,* immunofluorescence staining of PC-3 prostate tumors 6 wk after tumor implantation in mice showed different levels of PKC isozymes in tumor vessels. Representative immunostaining using anti-PKCα, βI, βII, ε antibodies (*red, top*), anti-CD31 antibodies (*green, middle*), and merged images (*yellow, bottom, arrowheads*) are shown (n = 5 each). *Scale bar,* 10 μm.

immunofluorescence experiments consisted of a Leica DMI 6000 B microscope with 350FX camera (JH Technologies).

Immunoblot analysis. Frozen tumors and livers were weighed, and two volumes of homogenization buffer [20 mmol/L Tris-HCl (pH 7.5), 2 mmol/L EDTA, 10 mmol/L EGTA, 250 mmol/L sucrose, 1:300 protease inhibitor cocktail (Sigma), and 1:300 phosphatase inhibitor cocktail (Sigma)] were added. The tissue was homogenized and was fractionated by spinning at 100,000 *g* for 30 min at 4°C. The supernatants correspond to the cytosolic fractions. The particulate fractions correspond to the rest of the intracellular organelles including nuclear and plasma membrane. The particulates were resuspended in homogenization buffer with 1% Triton X-100, and both detergent soluble and insoluble fractions were analyzed together. Translocation of PKCα, βI, βII, and ε was determined in cytosolic and particulate fractions from tumor and liver samples as described (26). Whole cell lysates refer to total homogenates without fractionation. For all PKC detections, 10 μg of whole cell lysates, cytosolic, and particulate fractions were used. Antibodies against GAPDH (1:10,000) and Gαi-3 (1:1,000) were used as loading controls for cytosolic and particulate fraction, respectively.

Kinase assay after immunoprecipitation. Tumor lysates were subjected for immunoprecipitation using PKCβII according to Chen and colleagues (19), and the immunoprecipitate was assayed for kinase activity in the absence of PKC activators (30).

Immunohistochemistry. Tissue sections in the slides were deparaffinized with xylene, hydrated by using a diluted alcohol series, and immersed in 3% H_2O_2 in distilled water for 15 min to quench endogenous peroxidase activity. The sections were then microwaved in a pressure cooker (Nordic Ware) for 30 min in distilled water containing 1 mmol/L EDTA. To avoid nonspecific staining, each section was incubated with 4% bovine serum albumin (Qbiogene) in PBS with 0.1% Tween 20 for 30 min at room temperature. The sections were then incubated with rabbit antipericentrin polyclonal antibody (4b; dilution: 1:250) in TBST [50 mmol/L Tris (pH7.5), 150 mmol/L NaCl, and 0.5% Tween 20] containing 4% Tryptone casein (Amresco) for 1 h at room temperature. Horseradish peroxidase (HRP)-conjugated secondary antibody against rabbit immunoglobulins (DAKO) was applied for 20 min at room temperature. Signals were amplified by catalyzed reporter deposition tyramine signal amplification (CSA II kit; DAKO), following the manufacturer's instructions. Each section was incubated with fluorescyl-conjugated tyramide for 15 min and protected from light. Sections were then incubated with HRP-conjugated anti-fluorescein antibody for 15 min at room temperature. Each step was followed by three successive rinses with TBST for 5 min. The chromogen used was 3,3′-diaminobenzidine (DAKO). Sections were counterstained in Meyer's hematoxylin.

Statistical analysis. Data are expressed as mean ± SE. Paired *t* test and repeated ANOVA were used to assess significance ($P < 0.05$).

Results

High levels of PKCβII are present in growing tumors and in the tumor endothelium. Because PKC activation has been implicated during growth of various tumors (31, 32), we first determined which PKC isozyme is present in growing PC-3 human prostate cancer cells in a xenograft model, *in vivo*. PKCα, βI, βII, and ε were all found in the PC-3 tumors (Fig. 2*A*). We next compared the cellular distribution of the PKC isozymes in the PC-3 xenografts with that in a primary culture of normal human prostate epithelial cells (PEC). We used the cellular distribution of the isozymes in PEC as a measure of basal levels of PKC activation (Fig. 1*A, left*; cytosolic enzyme represents inactive PKC; ref. 33). All the PKC isozymes were more active in the PC-3 xenografts relative to the primary PEC, and PKCβII seemed more active relative to the other isozymes, as evidenced by high levels of this isozyme in the particulate fraction relative to the cytosolic fraction. This was also apparent when comparing PKCβII and its alternatively spliced form, PKCβI ($n = 4$ each; $P = 0.01$; Fig. 1*A, right*). Immunofluorescence studies showed that PKCβII was more localized to endothelial cells relative to PKCα, βI, or ε (Fig. 1*B, arrowheads*). Based on these results, we focused our study on determining the role of PKCβII in angiogenesis and in tumor growth.

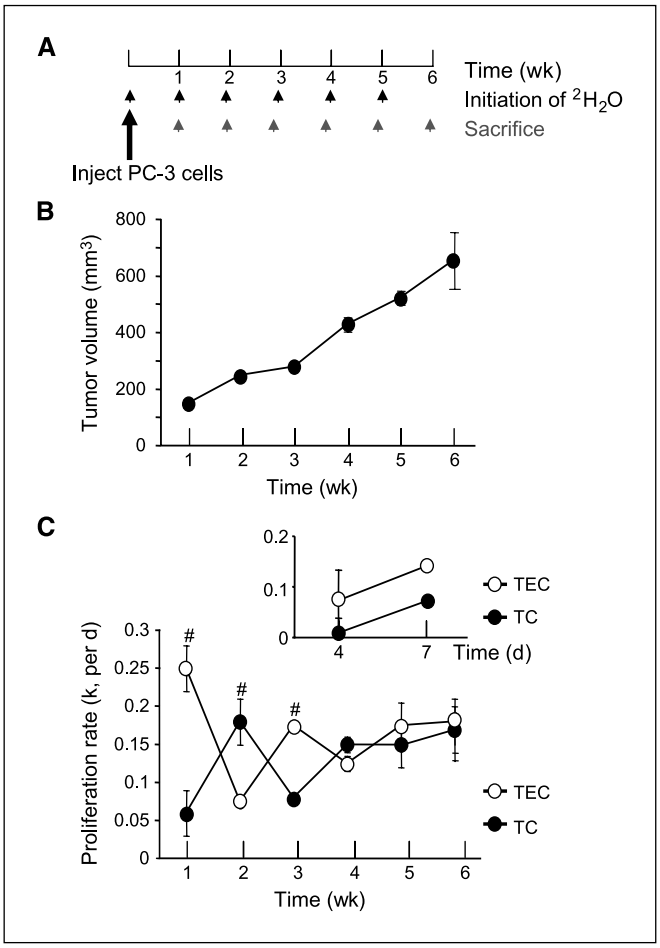

Figure 2. In the early phase of tumor growth, an increase in endothelial cell proliferation rate precedes that of the TCs. *A,* PC-3 TCs (5×10^6 cells) were injected s.c. into the left flank and the xenograft tumors were isolated each week up to 6 wk after tumor implantation. Deuterated water was administered via i.p. injection (8%) and in the drinking water (4%) for 1 wk before each study. *B,* tumor volume of PC-3 xenografts from week 1 to 6 after TC injection was measured using a caliper; *Points,* mean; *bars,* SE. *C,* proliferation rates of isolated TECs (*open circle*) and TCs (*filled circle*) were analyzed by GC-MS ($n = 4$–7 per week). Different cell populations were isolated using FACS (see Supplementary Fig. S1). Proliferation rate [i.e., fractional turnover rate (*k*) per day] was calculated as previously described (28, 29). Repeated ANOVA was used to determine the significance of differences between the curves. A two-tailed Student's *t* test and ANOVA were used to determine the differences ($P < 0.005$, repeated ANOVA; #, $P < 0.05$, Student's *t* test). *Insert,* the xenograft tumors were grown for 4 and 7 d after TC injection and TECs and TCs were obtained to measure their proliferation rates. Deuterated water was administered for 4 d before sacrifice ($n = 6$–10 per time point).

Increase in proliferation rate of TECs precedes that of tumor cells. To examine the proliferation kinetics of tumor cells and endothelial cells in the growing tumor, we used a new method that measures directly the proliferation rates of these cells, *in vivo* (Fig. 2*A*–*C*). PC-3 cancer cells were injected s.c. (5×10^6 cells) into the flank area of male nude mice and the resulting solid tumors were isolated each week, for up to 6 weeks after tumor cell injection (Fig. 2*A* and *B*). For each time point, deuterated water was administered in drinking water for 1 week before sacrificing,

and the TECs and tumor cells were isolated by fluorescence-activated cell sorting (FACS). The proliferation rate of each cell type was calculated by measuring the amount of deuterium in the DNA of these cells, as we previously described (28, 29).

Interestingly, the rise in TEC proliferation rate preceded the increase in the proliferation rate of the TCs during the first 4 weeks (Fig. 2*C*); rates of proliferation of these two cell types continued to change in an oscillating pattern for ~4 weeks. These data support the predicted coordination between tumor growth and angiogenesis with TEC proliferation and angiogenesis rising to meet the metabolic demand of the growing tumor (4, 34). After week 4, the TEC and TC proliferation rates seemed to reach a steady-state, suggesting that the rate of angiogenesis had matched the metabolic demand of the growing tumor (4, 34). We further examined the kinetics of cell proliferation during the days 0 to 7 of posttumor injection (n = 6–10 animals each, *insert*). The proliferation rate of TECs was severalfold higher than that of TCs during day 0 to 4 and days 4 to 7 (Fig. 2*C, insert*), indicating active tumor angiogenesis during the early period of tumor growth with only moderate TC proliferation at that period. This confirms that angiogenesis is particularly active in the early period of tumor growth and suggests a window of treatment for antiangiogenesis.

A PKCβII-specific inhibitor effectively reduced PC-3 tumor growth rate. Because we found PKCβII to localize mainly in endothelial cells, we next determined its role in tumor growth and angiogenesis, *in vivo*. We implanted osmotic pumps with saline, control peptide (TAT_{47-57} carrier peptide; refs. 35, 36) or βIIV5-3 (PKCβII-selective inhibitor peptide) conjugated to TAT_{47-57} to deliver the PKCβII inhibitor (25) into the cells. Specifically, 1 week after injection of the PC-3 cells, mice were implanted with osmotic pumps with saline/TAT or βIIV5-3 at 3.6 mg/kg/day for 2 weeks followed by 36 mg/kg/day for the following 3 weeks. Already after 2 weeks of treatment, there was a trend toward decreased tumor size in the βIIV5-3–treated animals (Fig. 3*A*). When the βIIV5-3 concentration was increased from 3.6 to 36 mg/kg/day for the next 3 weeks (a dose that was well-tolerated; ref. 37), tumor volume was found to be significantly smaller in the βIIV5-3–treated group over time (Fig. 3*A*, repeated ANOVA; *, $P < 0.05$; n = 4–5 each). Previous *in vivo* studies showed that inhibition of PKC translocation by systemic peptide delivery was observed in all tissues (26). Similarly, we found here that βIIV5-3 treatment reduced the level of PKCβII in the particulate fraction relative to the cytosolic fraction in tumor as well as in other tissues e.g., in liver (βIIV5-3 treatment decreased PKCβII translocation by 25–35%; Fig. 3*B, right*; $P < 0.05$; n = 3 each). We have previously shown that such a decrease in PKC translocation is sufficient to inhibit its pathologic activity (e.g., refs. 38, 39). We further confirmed the selectivity of the PKCβII inhibitor; sustained treatment of βIIV5-3 did not affect

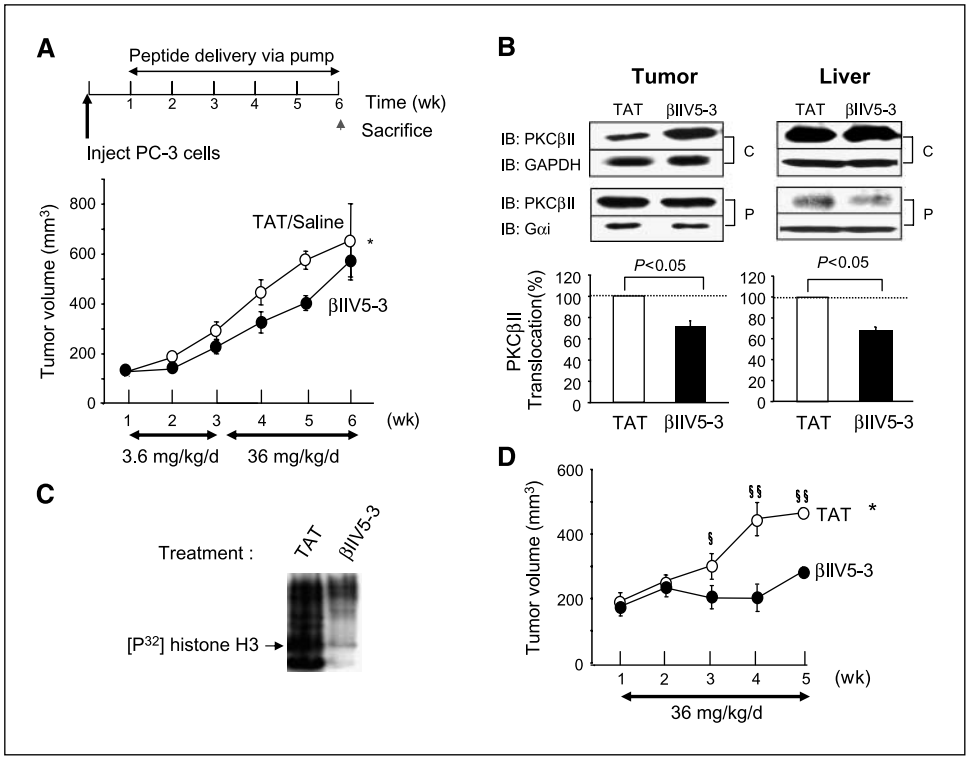

Figure 3. PC-3 tumor growth rate was reduced with PKCβII-specific inhibitor treatment. One week after PC-3 cell injection, mice were implanted with osmotic pumps with saline, control peptide (Twas administered for 1 wk before sacrifice. *A,* tumor volume was measured weekly (repeated ANOVA; *, $P < 0.05$; n = 4–5 each). Tumors were excised and weighed at week 6. Final tumor weight was 40% lower in the βII V53–treated group, but this difference did not reach statistical significance and there was no difference in body weight between the groups. *B,* 5-wk continuous βIIV5-3–treatment decreased PKCβII translocation to the particulate fraction of both tumors and livers. The active level of PKCβII was analyzed by Western blot after fractionation. GAPDH and Gαi were used as loading controls for the cytosolic and particulate fractions, respectively. *IB,* immunoblot. A two-tailed Student's t test was used to determine significance (n = 3 each, $P < 0.05$). *C,* βIIV5-3 treatment in vivo results in reduced PKC kinase activity as measured in vitro, after immunoprecipitation with anti-PKCβII antibodies. Kinase assay was performed in the absence of added PKC activators, using histone (*H3*) as a substrate as described (30). The film was exposed for 3 d in −80°C. *D,* a greater decrease in PC-3 tumor growth rate was obtained with a higher dose of βIIV5-3 (36 mg/kg/d for 4 wk). A repeated ANOVA and a two-tailed Student's t test was used to determine significance (*, $P < 0.05$ in repeated ANOVA; §, $P < 0.05$ versus TAT treated; §§, $P < 0.005$ versus TAT treated in Student's t test; n = 8–9 each; 16% versus 60% reduction in the overall tumor growth rate; *A* versus *D*). Additional blots for *B* and *C* are provided in Supplementary Fig. S2.

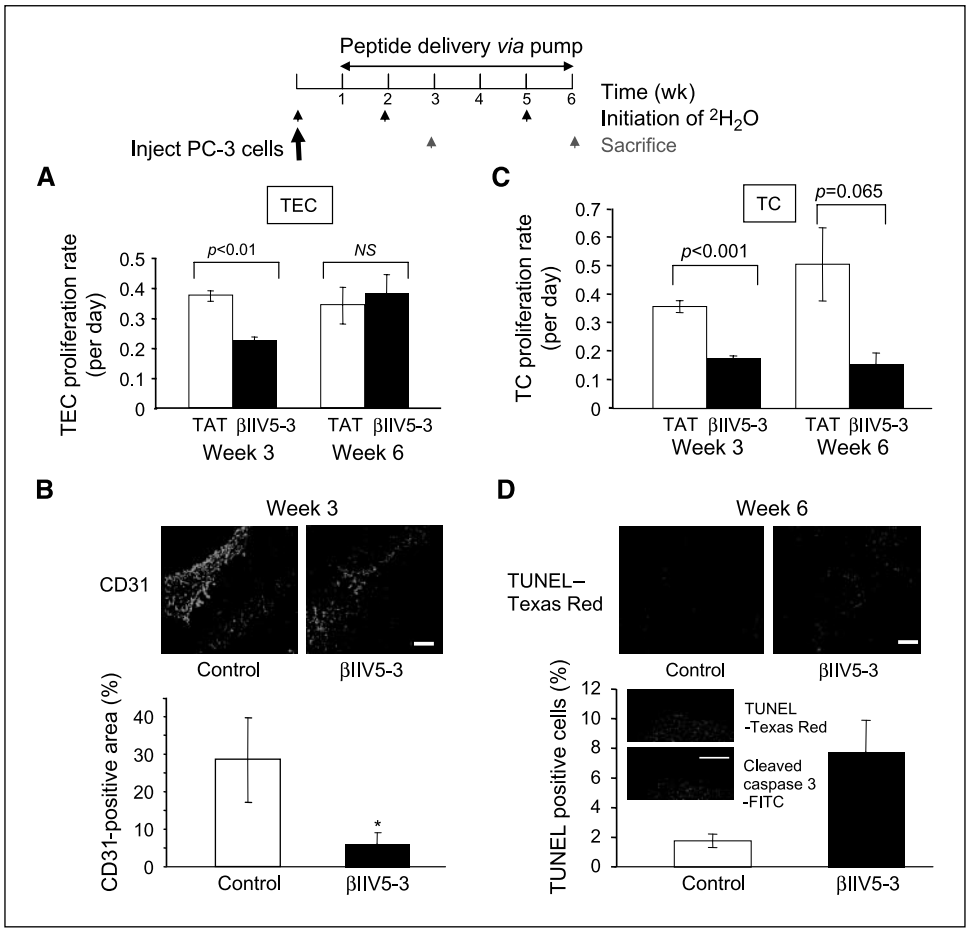

Figure 4. Analysis of proliferation rates of TECs and TCs after peptide treatment. *A,* mice treated with βIIV5-3 at 3.6 mg/kg/d for 2 wk and with 36 mg/kg/d for the remaining 3 wk were sacrificed at week 3 (midpoint), and at the end of the treatment at week 6, and the proliferation rates of TECs were then determined after their isolation. Deuterated water was administered during the 7 d before sacrifice. A two-tailed Student's *t* test was used to determine significance (*A*; $P = 0.008$ at week 3; $n = 8–9$ each). *B,* tumor sections from week 3 and 6 were stained with CD31-FITC antibodies, and immunostaining intensity was quantified using Photoshop. A two-tailed Student's *t* test was used to determine significance (*B,* week 3 data; *, $P < 0.05$). *Scale bar,* 10 μm. *C,* mice treated with βIIV5-3 at 3.6 mg/kg/d for 2 wk and with 36 mg/kg/d for the remaining 3 wk were sacrificed at week 3 (midpoint) and at the end of the treatment at week 6 to isolate and determine proliferation rates of TCs. A two-tailed Student's *t* test was used to determine significance (*C,* $P = 0.0007$ at week 3; $n = 8–9$ each). *D,* tumor sections from week 3 and 6 were stained for TUNEL conjugated with Texas red (*D,* week 6 data; $P = 0.06$; $n = 4$). TUNEL staining was confirmed with cleaved caspase 3 staining (FITC conjugated) of 3-wk tumor samples (*insert*). *Scale bars,* 10 μm.

translocation of the closely related PKCβI in the tumor nor PKCε in the liver (Supplementary Fig. S2). Using kinase assay in vitro in the absence of added PKC activators, we found that βIIV5-3 treatment resulted in an ~85% reduction in the catalytic activity of PKCβII immunoprecipitated from total tumor lysates containing equal amounts of protein (Fig. 3*C*), confirming sustained inhibition of PKCβII in the treated tumors.

We next set out to confirm the tumor growth inhibitory effect *in vivo* by administering βIIV5-3 at the higher dose of 36 mg/kg/day from week 1 to 5 (i.e., when we observed the most active angiogenesis; see Fig. 2*C*). This treatment decreased overall tumor growth rate by 60% compared with 16% with the lower dose of βIIV5-3, calculated as the change in tumor volume over time (Fig. 3*D*; $P < 0.05$, $n = 8–9$ each versus Fig. 3*A*).

βIIV5-3 decreased proliferation rates of TECs and TCs. Next, we determined whether βIIV5-3 affected cell division of TECs by directly measuring *in vivo* cell proliferation rates using deuterated water, as in Fig. 2. At week 3 with 2 weeks of sustained treatment with βIIV5-3 (3.6 mg/kg/day), TEC proliferation rates were reduced by 40%, compared with control mice (Fig. 4*A*; $P = 0.008$; $n = 8–9$ each). However, there was no difference in the proliferation rates 5 weeks after sustained treatment (at week 6) of βIIV5-3 (3.6 mg/kg/day followed by 36 mg/kg/day). These data suggest that the antiangiogenic effect of βIIV5-3 is more pronounced at the early stage of tumor growth, even at a lower dose. To confirm the antiangiogenic effect of βIIV5-3, tumor sections at week 3 and 6 were stained with anti-CD31 antibody, a marker of endothelial cells (Fig. 4*B*). There was a significantly lower number of CD31-positive tumor vessels in the βIIV5-3–treated samples compared with controls at week 3 (28% ± 11% versus 6% ± 3%; $P < 0.05$; Fig. 4*B*), but not at week 6 (not significant; data not shown), quantified using Photoshop program (Ver. 9.0.1).

βIIV5-3 treatment also decreased TC proliferation rates at week 3 ($P < 0.001$; Fig. 4*C*) and showed a trend for inhibition at week 6 ($P = 0.065$; Fig. 4*C*). Moreover, there was a stronger tendency of increased TUNEL-positive cells in the βIIV5-3–treated tumors at week 6 relative to TAT or saline controls (2% ± 1% versus 8% ± 2%; $P = 0.06$; Fig. 4*D*), compared with week 3 (not significant). We found that TUNEL-positive cells overlapped with staining for cleaved caspase 3 (Fig. 4*D, insert*), further confirming an increase in apoptosis. This suggests that at an earlier tumor stage, βIIV5-3 treatment decreases cell proliferation of both the TECs and TCs rather than inducing apoptosis.

βIIV5-3 treatment induced colocalization of PKCβII and pericentrin in PC-3 tumors. We next set out to determine the molecular basis for inhibition of tumor growth by βIIV5-3. An unbiased two-hybrid screen by Newton and collaborators (19) showed that a centrosomal protein, pericentrin, which is involved in controlling cytokinesis, microtubule organization, and spindle formation, binds PKCβII.

Pericentrin levels in human prostate cancer have been shown to be elevated with increasing Gleason grade (23, 40). Furthermore, pericentrin overexpression is associated with centrosomal defects leading to chromosomal instability, microtubule missegregation,

larger nuclei, and increased cell proliferation in human prostate and other types of cancer cells (23, 40–43). We therefore hypothesized that regulation of interaction of PKCβII with pericentrin may play a role in the phenotype that we observed. Pericentrin staining appears as a dot or two in normal cells (Supplementary Fig. S3; refs. 19, 23, 40). However, staining of the PC-3 tumor xenografts showed an abnormal pattern of pericentrin staining with elongated filamentous structures (Fig. 5*A, left*). Treatment with 36 mg/kg/day of βIIV5-3 for 4 weeks significantly reduced the abnormal filamentous pericentrin staining, reduced the overall staining intensity, and resulted in the return of a dotted staining pattern with antipericentrin antibodies (Fig. 5*A, right*). This was confirmed by Western blot analyses of pericentrin (~220 kDa) and its cleaved form (~150 kDa) in the total tumor lysate (Fig. 5*B*). The amount of cleaved form of pericentrin was reduced by ~90% with βIIV5-3 treatment compared with TAT controls (Fig. 5*B, bottom arrow*). We also found that enlongated and filamentous pericentrin did not colocalize with PKCβII in TAT-treated tumors (*; Fig. 5*C, 2–4*), whereas dotted pericentrin colocalized with PKCβII in βIIV5-3–treated tumors (*arrows*; Fig. 5*C, 6–8*). This was confirmed by determining the interaction between pericentrin and PKCβII *in vivo* by coimmunoprecipitation assay followed by Western blot analysis of the immunoprecipitate. PKCβII was immunoprecipitated from the total tumor lysate using anti-PKCβII antibodies and detected with antibodies against pericentrin (Fig. 5*D, top, lanes 2* and *3*). We detected pericentrin (~220 kDa) and its cleaved form (~150 kDa) in the immunoprecipitate (44, 45). Although the total level of pericentrin was lower in the βIIV5-3–treated group compared with the TAT-treated group (Fig. 5*B*), there was 10-fold more pericentrin associated with PKCβII compared with that associated in immunoprecipitates from TAT-treated tumors (Fig. 5*D, top, lanes 2*, and and *3*). Immunoprecipitate from the lysate of primary culture of

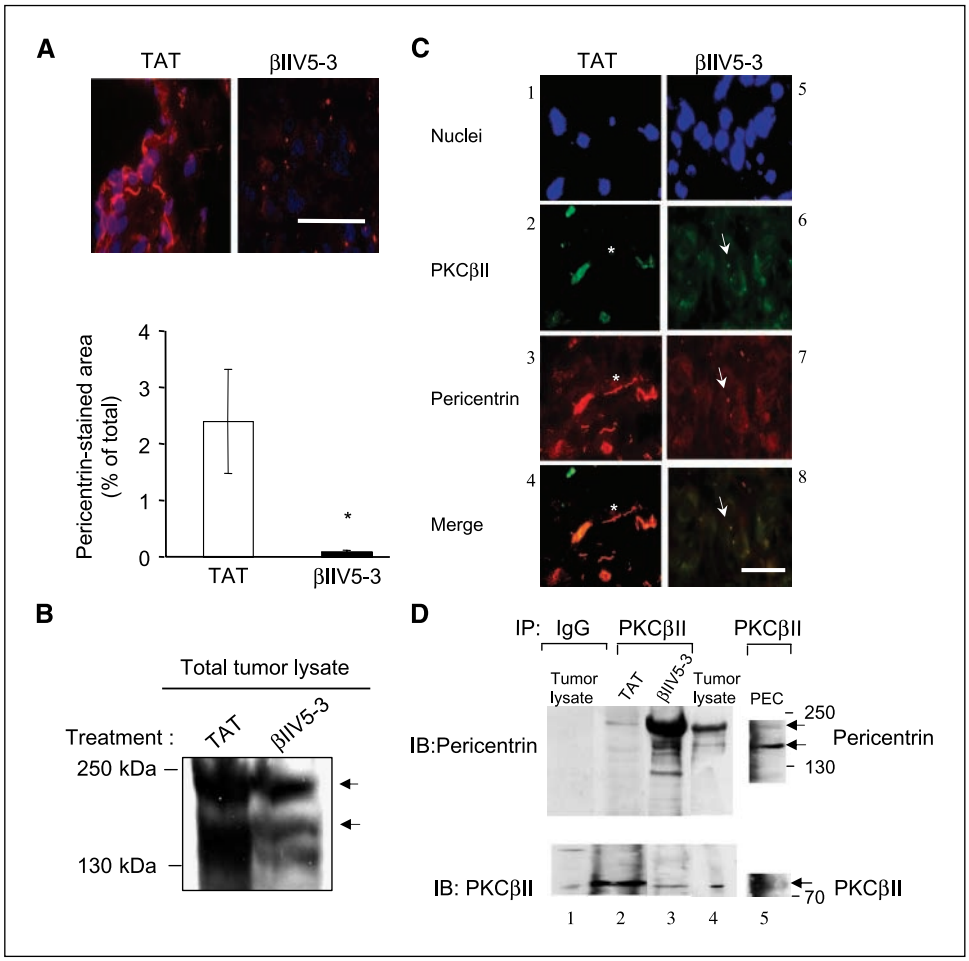

Figure 5. βIIV5-3 treatment reduced pericentrin levels and induced colocalization of PKCβII and pericentrin in PC-3 tumors. *A,* the level of pericentrin was determined using tumor sections after a 4-wk treatment with TAT or βIIV5-3 at 36 mg/kg/d. Sections were stained for pericentrin (rabbit polyclonal Ab4448; Abcam; followed by goat anti-rabbit conjugated to Cy3; *pink*) and for nuclei (Hoechst; *blue*). *B,* the levels of both the 220- and 150-kDa bands corresponding to pericentrin (*arrows*; refs. 22, 44, 45) were determined using total tumor lysates after a 4-wk treatment with TAT or βIIV5-3 at 36 mg/kg/d. *C,* immunofluorescence staining of 4-wk–treated tumors showed colocalization of PKCβII and normal dot-structured pericentrin in βIIV5-3–treated tumors. Shown are nuclei staining (*1* and *5*), PKCβII (*2* and *6*; *green*), pericentrin (*3* and *7*; *red*), and merged figure (*4* and *8*). *Arrows,* colocalization of pericentrin and PKCβII (*yellow*); *, filamentous pericentrin not colocalized with PKCβII. *D,* the interaction of PKCβII and pericentrin was further confirmed by immunoprecipitation (*IP*). Immunoprecipitates from the detergent-solubilized total tumor lysate and PECs using anti-PKCβII antibody were immunoblotted with the mixture of 4b, M1, and UM225 pericentrin antibodies (19) to detect pericentrin (*D, top, lanes 2, 3*, and *5, arrows*). Both the 220- and 150-kDa bands corresponding to pericentrin (22, 44, 45) were present in immunoprecipitates, showing that they interact with PKCβII *in vivo*. The interaction with PKCβII was stronger with βIIV5-3 treatment (compare *top, lanes 2* and *3*). In the negative control (*lane 1*, incubated with IgG and immunoprecipitated with beads), the amount of pericentrin (*top, lane 1*) or PKCβII (*bottom, lane 1*) present was not significant. Whole tumor lysates of tumor was used as a positive control (*lane 4*) to show pericentrin and PKCβII bands (*top* and *bottom, lane 4*). Also, immunoprecipitate from the lysate of primary culture of PECs that were not treated with βIIV5-3 was used to show interaction of PKCβII and pericentrin in normal prostate cells (*lane 5*).

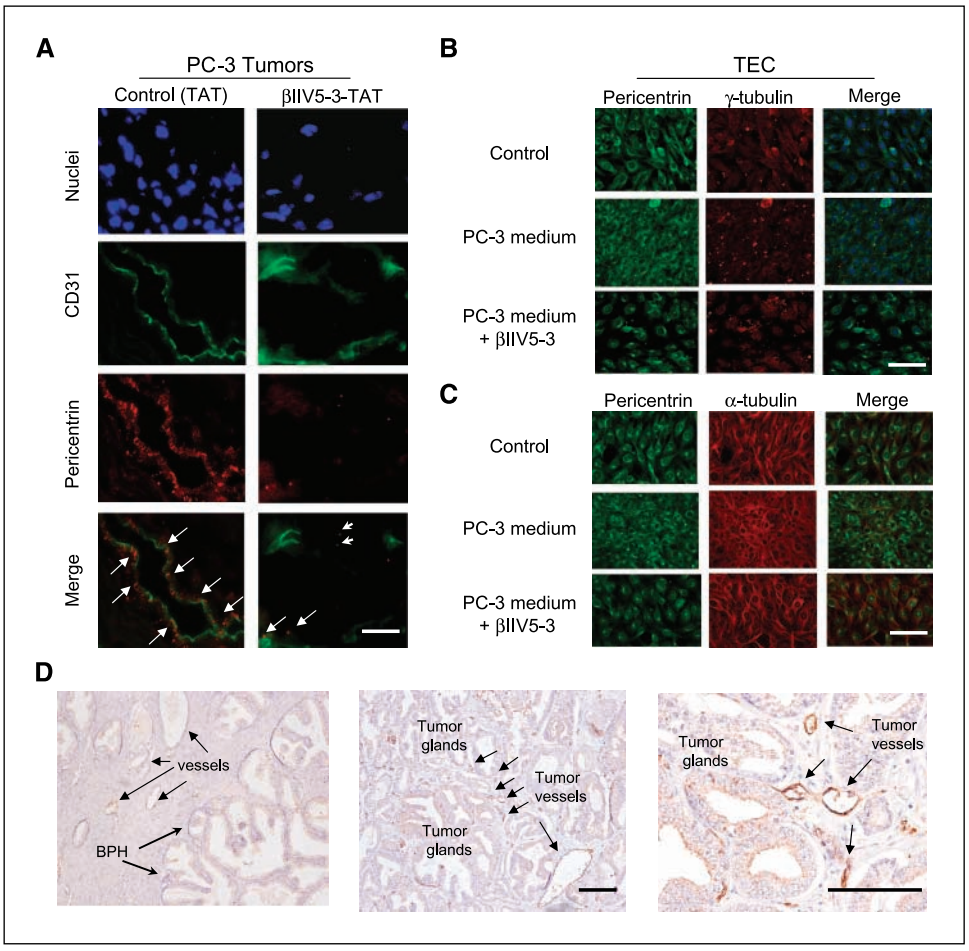

Figure 6. Pericentrin abnormality is present in TECs and in human tumor endothelium. *A,* tumor sections from mice treated for 4 wk with TAT or βIIV5-3 (36 mg/kg/d) were stained for nuclei (Hoechst), CD31 (*green*), and pericentrin (*red*). *Scale bar,* 10 μm. *B,* the presence of abnormal pericentrin and centrosomal defects in TECs grown in PC-3–conditioned medium was determined by immunofluorescence. Mouse TECs were grown in DMEM or in PC-3–conditioned medium (medium from PC-3 cells grown for 2 d) and treated with TAT or βIIV5-3 at a final concentration of 1 μmol/L (added thrice per day for 2 d). Representative images of TEC grown in DMEM with TAT (*top*), in PC-3–conditioned medium with TAT (*middle*) and with βIIV5-3 (*bottom*) are shown (representative of three experiments). Tumor endothelial cells were stained separately for pericentrin (*green*) and γ-tubulin (*red*). Merged figures are also shown (including nuclei stained with Hoechst). *Scale bar,* 10 μm. *C,* staining with anti–α-tubulin suggests abnormal microtubule structure in the TECs. Tumor endothelial cells treated the same as in (*B*) were stained separately for pericentrin (*green*) and α-tubulin (*red*). Merged figures are also shown (including nuclei staining with Hoechst). *Scale bar,* 10 μm. *D,* the level of pericentrin is high in human prostate tumor endothelium. The level of pericentrin was determined using paraffin-embedded sections from human prostate with Gleason grades 3, 4, and 5 cancers and were stained for pericentrin and counterstained with hematoxylin. Representative pictures are shown ($n = 8$; *left,* pericentrin staining on endothelium adjacent to benign prostatic hyperplasia; *middle,* pericentrin staining on tumor endothelium adjacent to tumor glands with Gleason grades 3+4; *right,* magnified view of the middle figure). *Scale bars,* 10 μm.

PECs that were not treated with βIIV5-3 was also used to show interaction of PKCβII and pericentrin in normal human cells. The interaction between PKCβII and pericentrin was stronger than that in untreated PC-3 tumors (*lane 2* versus *5*).

Abnormal pericentrin staining in the TECs and in human tumor endothelium. Because we found that filamentous pericentrin was present in structures similar to microvessels (Fig. 5*A, left*), we costained tumor sections for CD31 (a marker of vessels) and pericentrin. In TAT-treated tumors, enlongated and filamentous pericentrin was seen in tumor vessels (Fig. 6*A, left, arrows*). In βIIV5-3–treated tumors, pericentrin staining was significantly reduced in tumor microvessels and dotted staining was apparent in both TCs (*arrowheads*) and tumor endothelium (Fig. 6*A, right, arrows*).

Because TECs are contributed by the mice, we used a mouse TEC line cultured in medium from PC-3 human cancer cells to simulate *in vivo* system (46). Medium from PC-3 cells increased the level of pericentrin staining in the endothelial cells (Fig. 6*B, left, middle row*) relative to those cultured in normal DMEM (Fig. 6*B, left, top row*). βIIV5-3 treatment reduced this effect (Fig. 6*B, left, bottom row*). To confirm that the pericentrin abnormality correlates with centrosomal defect, endothelial cells were also stained for γ-tubulin (Fig. 6*B, middle*). PC-3–conditioned medium increased the centrosomal γ-tubulin staining in the endothelial cells (Fig. 6*B, second, middle row*), whereas βIIV5-3 treatment normalized it similarly to TAT-treated cells (Fig. 6*B, second, bottom*, and *top rows*). Also, PC-3–conditioned medium resulted in disorganized forms of α-tubulin, representative of microtubule organization (Fig. 6*C, second, middle row*) in the endothelial cells, whereas βIIV5-3 treatment resulted in an organized form of microtubules, similar to TAT-treated cells in DMEM (Fig. 6*C, second column, bottom* and *top rows*).

To determine the clinical relevance of our findings, we assessed location and levels of pericentrin in prostate tissue from patients with Gleason grades 3, 4, and 5 cancers. Similar to our data in the xenograft model, in some patients, we found higher levels of

pericentrin in the cytoplasm of endothelial cells adjacent to tumor glands (×100; Fig. 6*D, middle*) compared with those among benign prostatic hyperplasia (×100; Fig. 6*D, left*). The figure on the right is showing a magnified view of the middle figure (*right*; ×400). In tumors of other patients, some TECs were strongly stained for pericentrin, whereas others were stained at similar levels to those seen in endothelial cells among normal glands. These data suggest that, at least in some patients with Gleason grades 3 and up prostate cancers, there is up-regulation of pericentrin levels and localization in tumor endothelium.

Discussion

Determining isozyme-specific roles of PKC in tumors has been hampered by a lack of isozyme-specific regulators for each PKC isozyme. Here, we show that isozyme-specific inhibition of PKCβII by βIIV5-3 reduces PC-3 tumor growth in a xenograft model by decreasing angiogenesis, TC proliferation, and normalizing pericentrin levels and subcellular localization.

First, we found an oscillatory pattern of increase in the proliferation rates of tumor endothelial and TCs. This *in vivo* interplay between the TECs and TC proliferation has not been reported and provides a new insight into the relationship between the tumor and microenvironment during prostate cancer progression. These findings also identified a possible time window for drug treatment to reduce angiogenesis and tumor growth. Our findings may relate to the alternate apoptotic waves of these two cells types in Lewis lung carcinoma xenografts with chemotherapy as evidenced by TUNEL staining (6, 34); both are likely reflecting the tight regulation of angiogenesis by the tumor, to match metabolic demand of the tumor mass.

Microvessel density, the most frequently used method to measure angiogenesis, is not without limitations (4); vessel density does not represent the angiogenic activity of the tumor. Rather, it represents local tumor metabolic burden expressed as vessel to tumor ratio (4). Also, this measurement is laborious and quite subjective (47). We therefore used ^2H_2O to label DNA *in vivo*. Our method accurately measures net *in vivo* proliferation (i.e., turnover) rates of the TCs and the endothelial cells separately during the ^2H_2O administration period (28, 29) by analyzing isolated endothelial cells and TCs from the tissue (see Supplementary Fig. S1).

PKC family members are known to mediate cytokinesis and cell proliferation by regulation of microtubule organization (19–21). Expression studies of pericentrin fragments in cultured cells showed a key role for pericentrin as a scaffold protein for PKCβII II in microtubule organization, spindle assembly, and chromosome segregation (19). Here, βIIV5-3 seemed to normalize centrosome defects and microtubule misalignment seen in TECs. Knockdown of pericentrin in TEC and PC-3 cells using siRNA resulted in decreased γ-tubulin staining and reduction in the number of cells, supporting our data (Supplementary Fig. S4*B* and *C*). Because centrosome aberration and microtubule misorganization are thought to be possible causes of aneuploidy and chromosomal instability in some types of cancer, including prostate cancer (40, 41), the role of PKCβII/pericentrin interaction in the molecular events leading to aberration in cytokinesis and chromosomal missegregation needs to be determined. The cleaved form of pericentrin was suggested to be involved in malignant transformation (44, 45). Increased binding of PKCβII to pericentrin, especially the cleaved form, may inhibit further carcinogenesis. The effect of βIIV5-3, which inhibits the binding of PKCβII to its RACK, a receptor for activated C kinase (25, 48), may leave more PKCβII available for binding with pericentrin at the centrosome. We also found increased staining of pericentrin in endothelial cells can be induced by PKCβII-activating factor(s) secreted from the TCs. Our data suggest that the secreted factor is unlikely to be vascular endothelial growth factor (see Supplementary Fig. S5); the role of other secreted factors from prostate cancer cells (e.g., transforming growth factor α, basic fibroblast growth factor, and insulin-like growth factor; ref. 3) remains to be determined.

The findings that pericentrin levels are greatly elevated in human prostate tumors relative to normal prostate tissue, which pericentrin levels correlate with the Gleason grade (23, 40) and our immunohistochemistry data of high levels of pericentrin, specifically in the tumor endothelium (Fig. 6*D*) of some patients suggest that correction of pericentrin abnormalities with a PKCβII inhibitor, such as βIIV5-3, may improve both antiangiogenic and antitumor therapy. It remains to be determined whether the catalytic activity of PKCβII plays a role in pericentrin regulation or whether its role is confined to simply anchoring pericentrin. Our data also suggest that a larger study of humans with prostate cancer is warranted, to assess the correlation between the levels of pericentrin in tumor endothelium and the Gleason grade of the cancer.

In conclusion, we show that an isozyme-specific inhibitor of PKCβII localization and function reduces tumor growth by reducing angiogenesis and TC proliferation in a human prostate cancer xenograft model. We determined the appropriate window of treatment by analyzing proliferation kinetics of TECs and TCs *in vivo* using a direct measurement of cell proliferation. PKCβII inhibition corrected pericentrin localization and reduced other abnormalities, especially in the tumor vessels. Overall, our results suggest that a PKCβII inhibitor may provide a useful adjuvant treatment to the current therapy for patients with prostate cancer (and perhaps for patients with other solid tumors) by inhibiting proliferation of both TECs as well as TCs in the early phase.

Disclosure of Potential Conflicts of Interest

D.M. Rosen is the founder of KAI Pharmaceuticals, Inc., a company that plans to bring PKC regulators to the clinic. However, none of the work described in this study is based on or is supported by the company. No potential conflicts of interest were disclosed.

Acknowledgments

Received 11/12/2007; revised 5/15/2008; accepted 6/4/2008.

Grant support: Public Health Service Grant Number CA09151 awarded by the National Cancer Institute, Department of Health and Human Services (J. Kim).

The costs of publication of this article were defrayed in part by the payment of page charges. This article must therefore be hereby marked *advertisement* in accordance with 18 U.S.C. Section 1734 solely to indicate this fact.

References

1. Nelson WG. Prostate cancer prevention. Curr Opin Urol 2007;17:157–67.
2. Walczak JR, Carducci MA. Prostate cancer: a practical approach to current management of recurrent disease. Mayo Clin Proc 2007;82:243–9.
3. Charlesworth PJ, Harris AL. Mechanisms of disease: angiogenesis in urologic malignancies. Nat Clin Pract Urol 2006;3:157–69.
4. Hlatky L, Hahnfeldt P, Folkman J. Clinical application of antiangiogenic therapy: microvessel density, what it does and doesn't tell us. J Natl Cancer Inst 2002;94:883–93.
5. Folkman J. The role of angiogenesis in tumor growth. Semin Cancer Biol 1992;3:65–71.

6. Browder T, Butterfield CE, Kraling BM, et al. Antiangiogenic scheduling of chemotherapy improves efficacy against experimental drug-resistant cancer. Cancer Res 2000;60:1878–86.

7. Burdelya LG, Komarova EA, Hill JE, et al. Inhibition of p53 response in tumor stroma improves efficacy of anticancer treatment by increasing antiangiogenic effects of chemotherapy and radiotherapy in mice. Cancer Res 2006;66:9356–61.

8. Faivre S, Djelloul S, Raymond E. New paradigms in anticancer therapy: targeting multiple signaling pathways with kinase inhibitors. Semin Oncol 2006;33:407–20.

9. Griner EM, Kazanietz MG. Protein kinase C and other diacylglycerol effectors in cancer. Nat Rev Cancer 2007;7: 281–94.

10. Das Evcimen N, King GL. The role of protein kinase C activation and the vascular complications of diabetes. Pharmacol Res 2007;55:498–510.

11. Montesano R, Orci L. Tumor-promoting phorbol esters induce angiogenesis *in vitro*. Cell 1985;42:469–77.

12. Takahashi T, Ueno H, Shibuya M. VEGF activates protein kinase C-dependent, but Ras-independent Raf-MEK-MAP kinase pathway for DNA synthesis in primary endothelial cells. Oncogene 1999;18:2221–30.

13. Castagna M, Takai Y, Kaibuchi K, Sano K, Kikkawa U, Nishizuka Y. Direct activation of calcium-activated, phospholipid-dependent protein kinase by tumor-promoting phorbol esters. J Biol Chem 1982;257:7847–51.

14. Graff JR, McNulty AM, Hanna KR, et al. The protein kinase Cβ-selective inhibitor, Enzastaurin (LY317615.HCl), suppresses signaling through the AKT pathway, induces apoptosis, and suppresses growth of human colon cancer and glioblastoma xenografts. Cancer Res 2005; 65:7462–9.

15. Teicher BA, Alvarez E, Menon K, et al. Antiangiogenic effects of a protein kinase Cβ-selective small molecule. Cancer Chemother Pharmacol 2002;49:69–77.

16. Teicher BA, Menon K, Alvarez E, Shih C, Faul MM. Antiangiogenic and antitumor effects of a protein kinase Cβ inhibitor in human breast cancer and ovarian cancer xenografts. Invest New Drugs 2002;20:241–51.

17. Koren R, Ben Meir D, Langzam L, et al. Expression of protein kinase C isoenzymes in benign hyperplasia and carcinoma of prostate. Oncol Rep 2004;11:321–6.

18. Green LJ, Marder P, Ray C, et al. Development and validation of a drug activity biomarker that shows target inhibition in cancer patients receiving enzastaurin, a novel protein kinase C-β inhibitor. Clin Cancer Res 2006;12:3408–15.

19. Chen D, Purohit A, Halilovic E, Doxsey SJ, Newton AC. Centrosomal anchoring of protein kinase C βII by pericentrin controls microtubule organization, spindle function, and cytokinesis. J Biol Chem 2004;279:4829–39.

20. Kiley SC, Parker PJ. Differential localization of protein kinase C isozymes in U937 cells: evidence for distinct isozyme functions during monocyte differentiation. J Cell Sci 1995;108:1003–16.

21. Takahashi M, Mukai H, Oishi K, Isagawa T, Ono Y. Association of immature hypophosphorylated protein kinase cε with an anchoring protein CG-NAP. J Biol Chem 2000;275:34592–6.

22. Doxsey SJ, Stein P, Evans L, Calarco PD, Kirschner M. Pericentrin, a highly conserved centrosome protein involved in microtubule organization. Cell 1994;76:639–50.

23. Pihan GA, Purohit A, Wallace J, Malhotra R, Liotta L, Doxsey SJ. Centrosome defects can account for cellular and genetic changes that characterize prostate.

24. Peehl DM. Human prostatic epithelial cells. In: Freshney RI, Freshney MG, editors. Culture of Epithelial Cells. New York: Wiley-Liss; 2002. p. 171–94.

25. Stebbins EG, Mochly-Rosen D. Binding specificity for RACK1 resides in the V5 region of β II protein kinase C. J Biol Chem 2001;276:29644–50.

26. Begley R, Liron T, Baryza J, Mochly-Rosen D. Biodistribution of intracellularly acting peptides conjugated reversibly to Tat. Biochem Biophys Res Commun 2004;318:949–54.

27. Inagaki K, Begley R, Ikeno F, Mochly-Rosen D. Cardioprotection by ε-protein kinase C activation from ischemia: continuous delivery and antiarrhythmic effect of an ε-protein kinase C-activating peptide. Circulation 2005;111:44–50.

28. Kim SJ, Cheung S, Hellerstein MK. Isolation of nuclei from label-retaining cells and measurement of their turnover rates in rat colon. Am J Physiol Cell Physiol 2004;286:C1464–73.

29. Neese RA, Misell LM, Turner S, et al. Measurement *in vivo* of proliferation rates of slow turnover cells by 2H2O labeling of the deoxyribose moiety of DNA. Proc Natl Acad Sci U S A 2002;99:15345–50.

30. Disatnik MH, Boutet SC, Lee CH, Mochly-Rosen D, Rando TA. Sequential activation of individual PKC isozymes in integrin-mediated muscle cell spreading: a role for MARCKS in an integrin signaling pathway. J Cell Sci 2002;115:2151–63.

31. Hofmann J. Protein kinase C isozymes as potential targets for anticancer therapy. Curr Cancer Drug Targets 2004;4:125–46.

32. Koivunen J, Aaltonen V, Peltonen J. Protein kinase C (PKC) family in cancer progression. Cancer Lett 2006; 235:1–10.

33. Kraft AS, Anderson WB, Cooper HL, Sando JJ. Decrease in cytosolic calcium/phospholipid-dependent protein kinase activity following phorbol ester treatment of EL4 thymoma cells. J Biol Chem 1982;257: 13193–6.

34. Folkman J. Angiogenesis and apoptosis. Semin Cancer Biol 2003;13:159–67.

35. Chen L, Wright LR, Chen CH, Oliver SF, Wender PA, Mochly-Rosen D. Molecular transporters for peptides: delivery of a cardioprotective εPKC agonist peptide into cells and intact ischemic heart using a transport system, R(7). Chem Biol 2001;8:1123–9.

36. Schwarze SR, Ho A, Vocero-Akbani A, Dowdy SF. *In vivo* protein transduction: delivery of a biologically active protein into the mouse. Science 1999;285:1569–72.

37. Koyanagi T, Noguchi, K, Ootani, A, Inagaki K, Robbins RC, Mochly-Rosen D. Pharmacological inhibition of ε PKC suppresses chronic inflammation in murine cardiac transplantation model. J Mol Cell Cardiol 2007;43:517–22.

38. Bright R, Raval AP, Dembner JM, et al. Protein kinase C δ mediates cerebral reperfusion injury *in vivo*. J Neurosci 2004;24:6880–8.

39. Murriel CL, Churchill E, Inagaki K, Szweda LI, Mochly-Rosen D. Protein kinase Cδ activation induces apoptosis in response to cardiac ischemia and reperfusion damage: a mechanism involving BAD and the mitochondria. J Biol Chem 2004;279:47985–91.

40. Pihan GA, Wallace J, Zhou Y, Doxsey SJ. Centrosome abnormalities and chromosome instability occur together in pre-invasive carcinomas. Cancer Res 2003;63: 1398–404.

41. Nakajima T, Moriguchi M, Mitsumoto Y, et al. Centrosome aberration accompanied with p53 mutation can induce genetic instability in hepatocellular carcinoma. Mod Pathol 2004;17:722–7.

42. Neben K, Tews B, Wrobel G, et al. Gene expression patterns in acute myeloid leukemia correlate with centrosome aberrations and numerical chromosome changes. Oncogene 2004;23:2379–84.

43. Schneeweiss A, Sinn HP, Ehemann V, et al. Centrosomal aberrations in primary invasive breast cancer are associated with nodal status and hormone receptor expression. Int J Cancer 2003;107:346–52.

44. Golubkov VS, Chekanov AV, Doxsey SJ, Strongin AY. Centrosomal pericentrin is a direct cleavage target of membrane type-1 matrix metalloproteinase in humans but not in mice: potential implications for tumorigenesis. J Biol Chem 2005;280:42237–41.

45. Golubkov VS, Chekanov AV, Savinov AY, Rozanov DV, Golubkova NV, Strongin AY. Membrane type-1 matrix metalloproteinase confers aneuploidy and tumorigenicity on mammary epithelial cells. Cancer Res 2006;66: 10460–5.

46. Walter-Yohrling J, Morgenbesser S, Rouleau C, et al. Murine endothelial cell lines as models of tumor endothelial cells. Clin Cancer Res 2004;10:2179–89.

47. Baeten CI, Wagstaff J, Verhoeven IC, Hillen HF, Griffioen AW. Flow cytometric quantification of tumour endothelial cells; an objective alternative for microvessel density assessment. Br J Cancer 2002;87:344–7.

48. Vallentin A, Mochly-Rosen D. RBCK1, a protein kinase CβI (PKCβI)-interacting protein, regulates PKCβ-dependent function. J Biol Chem 2007;282:1650–7.